PCCP

Accepted Manuscript

ROYAL SOCIETY OF CHEMISTRY

www.rsc.org/pccp

Chirality-dependent structuration of protonated or sodiated polyphenylalanines: IRMPD and ion mobility studies

Valeria Lepere [a], Katia Le Barbu-Debus [a], Carine Clavaguéra [b], Debora Scuderi [c], Giovanni Piani [a], Anne-Laure Simon [e], Fabien Chirot [d], Luke MacAleese [e], Philippe Dugourd [e] Anne Zehnacker [a 1].

[a] Institut des Sciences Moléculaires d'Orsay (ISMO), CNRS, Univ. Paris-Sud, Université Paris-Saclay, F-91405 Orsay (France)

[b] LCM, CNRS, Ecole polytechnique, Université Paris-Saclay, 91128 Palaiseau, France

[c] Laboratoire de Chimie Physique (LCP), CNRS UMR 8000, Univ. Paris-Sud, F-91405 Orsay, France

[d] Université de Lyon, Univ Lyon 1, ENS de Lyon, CNRS, Institut des Sciences Analytiques, UMR 5280, F-69100 Villeurbanne, France,

[e] Université de Lyon, Univ Lyon 1, CNRS, Institut Lumière Matière, UMR 5306, F-69100 Villeurbanne, France.

Abstract

Ion mobility experiments are combined with Infra-Red Multiple Photon Dissociation (IRMPD) spectroscopy and quantum chemical calculations for assessing the role of chirality in the structure of protonated and sodiated di- or tetra-peptides. Sodiated systems show a strong chirality dependence of the competition between Na^+…O and Na^+…π interactions. Chirality effects are more subtle in protonated systems and manifest themselves by differences in the secondary interactions such hydrogen bonds between neutral groups or those involving the aromatic rings.

[1] Corresponding author anne.zehnacker-rentien@u-psud.fr

Introduction

Chirality has ubiquitous effects in chemistry, both at the microscopic and macroscopic levels. The desire of studying these effects without the perturbation brought by the environment has prompted several gas-phase approaches. Isolated weakly bonded diastereomers resulting from the non-covalent association of two chiral molecules have been the subject of numerous studies.[1] They include spectroscopic studies of neutral complexes in supersonic-jet conditions[2-11] and that of ionic species by mass spectrometry, with methods ranging from collision-induced dissociation[12], to the kinetic method or its variant,[13-15] ion-molecule reactions,[16, 17] or ion mobility[18, 19]. A few studies coupling spectroscopy and mass spectrometry have also been reported.[20-24] In contrast, spectroscopic studies of the differences between diastereomers isolated in the gas phase are scarce, despite their interest.[25-32] Indeed, diastereomers often possess different macroscopic chemical and biological properties, which stem from both different intra and intermolecular interactions. For example, the effect of ephedrine on blood pressure modification is twice that of pseudo ephedrine.[33] The two molecules also show microscopic differences, both in the number of populated conformers in jet-cooled conditions and in the strength of their intramolecular hydrogen bond.[34] The two diastereomers of an amino-alcohol, namely, (1R,2S) and (1R,2R)-amino-indanol, differ in their melting points (118°C vs. 142°C) because the former involves an intramolecular hydrogen bond and the latter does not.[29]

Of special interest is the comprehension of the way diastereomerism impinges the structure of biopolymers such as proteins.[35] While all the naturally-occurring aminoacids are L, post translational modifications can invert chirality, which has possible consequences on their structure and function. For example, reversal of chirality of a single amino-acid in the Trp-cage dication leads to structural modifications of its gas-phase structure detected by Electron Capture Dissociation (ECD).[36] Also in isolated peptides of more limited size, inverting the chirality of a residue may modify the intramolecular interactions hence the structure. This has been observed in capped neutral dipeptides showing a γ turn, which exists in two opposite handednesses whose relative stability is dictated by the chirality of the residues.[30] However, the chirality-induced structural changes seem to be limited in small peptides. While the reversal of chirality of one amino-acid unit in long protonated poly-alanine strands is sufficient to disrupt the helical shape adopted in the peptide when all the residues are of the same chirality,[37] no difference has been observed between protonated or

neutral LL and LD diphenylalanines.[25, 38, 39] In contrast, a marked chirality effect has been observed in the binding pattern between the same dipeptide and Li^+ or Na^+. [39] The observed binding motifs involve coordination of the alkali to the N-terminus aromatic ring, to the amide oxygen, and to one of the termini oxygens. While coordination to either of the termini has been proposed for LL, interaction with the carboxyl oxygen has been suggested to be energetically preferred in LD. The aim of this work is to extend the study of Dunbar *et al.* on diphenylalanines to tetraphenylalanines, either isotactic LLLL or syndiotactic LDLD. The question raised is whether chirality-induced structural differences also appear in the protonated forms when the sequence is longer. The aromatic character of the phenylalanine residue is expected to modify the competition between the strong electrostatic interaction between the cation and the peptide on the one hand, and the internal stabilization of the peptide on the other hand. Indeed, the aromatic rings can compete with C=O or N as a solvation site; they will increase stabilizing dispersion interactions within the peptide, and may intervene through the formation of NH…π hydrogen bonds[40] which have been shown to play an important role in chiral recognition.[11, 22] Reversal of the chirality of one or several residues can modify the subtle balance between these different intra and intermolecular forces.

To this end, we combine two technical approaches, namely Infra-Red Multiple Photon Dissociation (IRMPD) and Ion Mobility Spectrometry (IMS). IRMPD is a very powerful technique for the structural characterization of ions in the gas phase. It has been applied to protonated peptides such as Gly_n or Ala_n for which several binding sites have been suggested.[41-45] The interaction between alkali and Gly_n, Ala_n or Phe_2 has been the subject of numerous experimental and theoretical studies, with the aim of understanding the binding motif of the cation, either fully solvated by oxygen atoms or interacting also with one of the nitrogens.[38, 46-50]

However, IRMPD mainly probes the hydrogen bond network at play in these systems. In the polyphenylalanines studied here, the position of the phenyl rings is not directly probed by the IR. A method sensitive to the global shape of the molecule is therefore highly desirable. IMS provides information on the 3D structure of charged biomolecules in the gas phase.[51-53] Since the pioneering works of Bowers, Jarrold and Clemmer, numerous studies have been undertaken on systems, ranging from peptides[37, 52, 54] and DNA strands[55] to isolated proteins and complexes[56-58]. These two methods (IRMPD and IMS) nicely complement each other as global information on the molecular shape extracted from ion mobility is combined with local information about the hydrogen bond network inferred from the IRMPD results.

Such a dual approach was proposed already to probe the charge-solvated structure of guanidiniocarbonylpyrrole derivatives[59] or to study the structural properties of metal-peptide complexes.[60 61]

We present here a study of the influence of chirality on the structure of protonated (denoted H^+ in what follows) or sodiated (denoted Na^+ in what follows) isotactic or syndiotactic di- or tetra-phenylalanines, obtained by combining the results of IRMPD spectroscopy, ion mobility and quantum chemical calculations. Figure 1 schematically shows the studied molecules, with the chiral centers denoted by *. The peptides L-Phe-L-Phe, L-Phe-D-Phe, L-Phe-L-Phe-L-Phe-L-Phe and L-Phe-D-Phe-L-Phe-D-Phe will be denoted LL or LD and LLLL or LDLD, respectively.

Experimental and theoretical methods

LL or LD diphenylalanines and LLLL or LDLD tetraphenylalanines were purchased from GeneCust-Luxembourg and used without further purification. Protonated or sodiated ions were produced by Electrospray Ionization (ESI) of 500 µM peptides solutions prepared by dissolving the polypeptides in a H_2O/MeOH 50:50 mixture.

I. IRMPD spectroscopy

IRMPD spectra were obtained through MS^2 experiments by means of two set-ups. The first one was a modified Paul ion trap (Bruker, Esquire 3000+)[62] equipped with a Diamond entrance window and coupled to a Free Electron Laser (FEL) at the Centre Laser Infrarouge d'Orsay (CLIO). The FEL was focused by a 350 mm focal length ZnSe lens. IR spectra were obtained by mass selecting the precursor ions in a 2 Da window, with 300 ms irradiation time. Mass spectra were recorded after six accumulations, and the photon energy was scanned by steps of 4–5 cm^{-1}. The second set up involved a 7T Fourier transform ion cyclotron resonance (FT-ICR) hybrid mass spectrometer (Bruker, Apex Qe).[63] The CLIO FEL IR beam was mildly focused by a 2000 mm Ag-protected spherical concave mirror, with a typical beam waist at the centre of the FT-ICR of the order of 1 mm diameter. The CLIO FEL operated at 25 Hz with 8 µs long bunch pulses containing 0.5-3 ps micropulses separated by16 ns. The spectral bandwidth (full width at half maximum FWHM) was about 7 cm^{-1} with pulse energy of 1600 to 900 mW from 900 to 2000 cm^{-1}. The wavelength calibration was ensured by simultaneously recording the spectrum of polystyrene and that of the studied system.

Infrared spectra were obtained by monitoring the fragmentation efficiency F= -ln(P/(F + P)) as a function of the IR wavelength, with F being the sum of the abundances of the fragment ions produced by IRMPD and P that of the parent ion.

II. Ion mobility

Mobility measurements were performed using a homemade 1 m long drift cell coupled to a commercial quadrupole time-of-flight (micro-qTOF, Bruker-Daltonics, Bremen, Germany, mass resolution 10 000), as previously described in details. [52]

Electrosprayed ions were introduced through a heated capillary (around 250°C) and accumulated in an hourglass-shaped ion funnel. Ion packets were periodically injected in the drift tube, across which they travelled, driven by a uniform electric field operated between 8.3 and 4.7 V cm^{-1}. The helium pressure in the tube was maintained at 12 Torr. A second ion funnel was used to focus the diffuse ion packet at the exit of the drift tube and to guide them to the transfer region of the mass spectrometer through a 0.7 mm diameter aperture. Ions were then conveyed to the orthogonal extraction region of the time-of-flight mass analyzer which is operated at 10 kHz. Mass spectra could eventually be recorded as a function of the drift time of the ions in the tube. Under the experimental conditions, this drift time was inversely proportional to the drift field, and proportional to the orientationnally-averaged momentum transfer cross section for ion drift gas collisions.[64] Absolute values for these collision cross sections could then be extracted from drift time measurements at different drift voltages across the mobility cell. Following this procedure, the uncertainty on the measured cross sections was estimated to be no more than 3%.

III. Theoretical methods

The di- and tetra-peptides studied here are shown in Figure 1. The atoms are numbered according to the residue they are contained in, starting from the N terminus. The ionic intramolecular hydrogen bonds involved in the protonated peptides will be named Cn according to the number of atoms contained in the ring. Additional interaction involving neutral hydrogen bonds will be called C'n. Complexes of the oligopeptides with sodium will be named after the nature of the interaction with the alkali, i.e. an interaction between sodium and the carbonyl oxygen, the nitrogen, or the aromatic ring will be called O, N, π, respectively. For example, a structure with Na^+ interacting with two carbonyl oxygens and an aromatic cloud will be called OOπ.

For all the studied systems, exploration of potential energy surface was performed combining two different force fields (OPLS-2005 and MMFFs) with the advanced conformational search implemented in the MacroModel program available in the Schrödinger package.[65] At the end of the conformational searching step, all the peptide structures with energy below 20 kJ/mol. were optimized within the frame of the DFT theory at the RI-B97D/TZVPP level. The most promising conformers in terms of energetics and spectroscopy were further optimized using the dispersion-corrected functional B3LYP-D3 associated to the TZVPP basis set. Based on previous studies,[66, 67] this method was chosen because it combines a good frequency description of the hybrid functional B3LYP [68] and inclusion of empirical dispersion corrections.[69, 70] Final relative energies have been confirmed at the RI-CC2/TZVPP level on the B3LYP-D3 geometries. The calculations were performed with the Turbomole 6.6 [71] and the Gaussian packages.[72] The vibrational spectra were simulated by convoluting the harmonic frequencies obtained at the same level of calculation by a Lorentzian line shape (FWHM 20 cm^{-1}). For comparison with IMS measurements, collision cross sections were also calculated for the selected conformers using the trajectory method described by Mesleh *et al.* [73]

Experimental results

I. Mass and CID spectra of polyphenylalanines

The mass spectra of protonated or sodiated di- and tetra-phenylalanines were recorded prior to spectroscopic studies (Figure 2). The same peaks with similar intensities appear in the mass spectrum of LLH^+ and LDH^+. The protonated monomer appears at *m/z* 313.4, the dimer at *m/z* 625.8 and the trimer at *m/z* 938.2. Fragments appear at *m/z* 120.4 and *m/z* 166.4.

The mass spectra of $LLLLH^+$ and $LDLDH^+$ differ much more from each other than those of the dipeptides do. They are dominated by the protonated monomer (*m/z* 607.7), and dimer (*m/z* 1214.4). The trimer (*m/z* 1821.1) as well as a doubly-charged trimer (*m/z* 911.1) and pentamer (*m/z* 1517.8) strongly contribute to the spectrum of $LDLDH^+$, but are hardly seen in $LLLLH^+$. The heterochiral system shows therefore much more clustering propensity. In contrast with that of $LDLDH^+$, the mass spectrum of $LLLLH^+$ shows extensive fragmentation. Complexation with sodium impurity is also observed as a weak contribution at *m/z* 335.4 for diphenylalanines and *m/z* 629.7 for tetraphenylalanines.

MS^2 Collision-Induced Dissociation (CID) spectra of LLH^+ and LDH^+ show several fragments. The main fragmentation path corresponds to carboxyl loss (m/z 268.4), y_1 fragment (m/z 166.4) and a_1 fragment (m/z 120.4). The peaks at m/z 295.4 and m/z 222.4

which correspond to the loss of water (m/z 295.4) and of the radical residue (Ph-CH_2•) (m/z 222.4) are about one order of magnitude less intense. $LLNa^+$ and $LDNa^+$ show the same fragments as LLH^+ and LDH^+, except the loss of water, with however very different relative intensities. y_1 is dominant while the intensity of the other fragments is one to two orders of magnitude smaller. The influence of the chirality of the residues manifests itself by a smaller efficiency for the carboxyl loss in $LLNa^+$ than $LDNa^+$.

The MS^2 CID spectra of $LLLLH^+$ and $LDLDH^+$ show the same fragments, though $LLLLH^+$ shows higher fragmentation efficiency than $LDLDH^+$. The spectra are dominated by the y_2 and b_2 fragments which correspond to the dissociation into two dipeptide moieties. The dominant channel is b_2/y_2 followed by b_3/y_3 then a_2. In contrast to what is observed for the protonated dipeptides, loss of water or carboxyl group is negligible. The relative intensity of the fragments is similar in $LLLLH^+$ and $LDLDH^+$ except the y_3 fragment which is more intense in $LLLLH^+$. CID of sodiated tetraphenylalanines mainly leads to the loss of sodium, which is not observed in our experimental set up. The other fragments amount to 1% of the parent intensity (y_3) or less (b_3, y_2, a_3). Loss of water is only present for $LLLLNa^+$.

II. IRMPD spectra of protonated LL and LD

The IRMPD spectra of protonated LL and LD recorded in the fingerprint region are shown in Figure 3. They are very similar and present several bands. The band around 1150 cm^{-1} is the signature of the carboxylic OH bend devoid of hydrogen-bonding interaction.[49] The band around 1400 cm^{-1} corresponds to the NH_3^+ umbrella motion, and that around 1530 cm^{-1} to the NH_3^+ scissoring motion. Last, the higher-energy features around 1700 and 1760 cm^{-1} are typical of the carbonyl and carboxyl CO stretching modes. The only difference between the LL and LD spectra is the higher intensity of the band at 1530 cm^{-1} in the former. The bands are listed in Tables S1 and S2 in the supplementary information.

These results can be compared to those of Dunbar et al.[39], who reported the IRMPD spectrum of protonated LL and LD recorded with a FT-ICR ion trap coupled with the FELIX IR free-electron laser. The two spectra are identical except for a band at 1100 cm^{-1} which is not present in the spectra reported here for either of the systems. The differences observed between the two set-ups might arise from different trapping conditions, leading to different temperatures and conformer populations. They might also come from different irradiation conditions, such as laser power, or spectral bandwidth, which influence in a different way the absorption of modes with different anharmonicity.[74]

III. IRMPD spectra of sodiated LL and LD

The IRMPD spectra of sodiated LL and LD are presented in Figure 4. The bands are listed in Tables S3 and S4 in the supplementary information. Strong bands appear around 1700 cm^{-1}, which are characteristic of the CO stretching modes. The features around 1540 cm^{-1} correspond to the NH bending modes and that around 1160 cm^{-1} to the carboxylic OH bend. Differences in the position of the bands appear for the two systems of different chirality. While the band at 1163 cm^{-1} in $LLNa^+$ is blue shifted by 8 cm^{-1} in $LDNa^+$, the bands at 1537 and 1754 for $LLNa^+$ are moved towards the red at 1526 and 1742 for $LDNa^+$. Finally, the major difference is a shoulder at 1780 cm^{-1} observed for $LLNa^+$, which is not present in $LDNa^+$. This observation is in agreement with the studies of Dunbar et al. and can be explained in terms of the coexistence of two conformers.[39] As mentioned for the protonated species, the intensity ratio and bandwidths observed here slightly differ from those previously reported, in particular the intensity ratio between the 1742 and 1780 cm^{-1} bands observed in $LLNa^+$. This observation suggests that the population distribution between the isomers is not the same in the two experiments.

The sodiated systems do not show any band at 1485 cm^{-1}, as expected when no NH_3^+group is present in the system. This observation proves unambiguously that formation of a zwitterion can be excluded.

IV. IRMPD spectra of protonated LLLL and LDLD

The IRMPD spectra of protonated tetraphenylalanines are presented in Figure 5 and the position of the bands is listed in Tables S5 and S6. Five different regions appear for $LLLLH^+$. The presence of three distinct CO stretching bands between 1600 and 1800 cm^{-1} suggests the existence of CO groups involved in three different interactions. Two strong peaks appear at 1440 and 1500 cm^{-1} in the NH_3^+ umbrella and NH_3^+ scissoring region. Last, the region of the OH bend shows a single feature at 1141 cm^{-1} band. The $LDLDH^+$ spectrum is less structured. A congested band appears around 1700 cm^{-1} for the CO stretch, suggesting that the carbonyls are in similar environments. The NH bend region shows a single band around 1550 cm^{-1}. Besides much less structured features in the NH bend and CO stretch regions in $LDLDH^+$, the main difference relative to $LLLLH^+$ is the presence of a band at 1241 cm^{-1} and the absence of that at 1141 cm^{-1}. It has to be stressed that the spectra of protonated tetrapeptides are much more sensitive to chirality than those of dipeptides.

V. IRMPD spectra of sodiated LLLL and LDLD

The spectra of the sodiated tetraphenylalanines are presented in Figure 6 and the bands are listed in Tables S7 and S8. They are dominated by two intense and broad bands around 1680 cm^{-1}, characteristic of the CO stretches, and around 1500 cm^{-1}, typical of the NH bending modes. The weak band at 1750 cm^{-1} corresponds to the carboxylic CO stretch and is abnormally weak, as frequently observed for this sort of systems.[75] This might be due to two reasons. First, the laser power strongly decreases in this range (it falls from ~1.6W at 900 cm^{-1} to 0.7W at 1800 cm^{-1}). Second, the main dissociation channel is the loss of Na^+, which is not observed in the experimental set-up used. This might affect the relative intensities of the band. The $LLLLNa^+$ and $LDLDNa^+$ only differ by the relative intensity of the 1680 cm^{-1} peak. As in the case of diphenylalanines, the absence of a band around 1450 cm^{-1} indicates that no zwitterion is formed.

VI. Ion mobility measurements

The experimental collision cross sections (Table 1) deduced from the IMS measurements for LLH^+, LDH^+, and $LLNa^+$ (119, 116, and 116 ± 3 Å², respectively) are very similar considering the experimental error bars. In contrast, the cross section of 124 ± 3 Å² measured for $LDNa^+$ is significantly higher.

Regarding the tetraphenylalanines, the experimental cross sections reported in Table 1 display a clear difference between the protonated systems, for which the cross section is 178 ± 3 Å², and the sodiated systems, which were found to show significantly higher cross sections (183 and 188 ± 3 Å² for $LLLLNa^+$ and $LDLDNa^+$ respectively). The protonated systems then appear to be more compact than the corresponding sodiated species. However no marked difference as a function of the residue chirality could be detected for the sodiated tetrapeptides.

Calculation results and attribution

I. Calculated structures of diphenylalanines

The assignment has been made on the basis of a good agreement between the experimental spectrum and that simulated from the calculated harmonic frequencies and between the measured and calculated values for the collision cross sections. Among the calculated structures that satisfy these conditions, we have kept those that are the most stable. The selected diphenylalanine structures are shown in Figure 7. Table 1 presents their calculated

cross sections and relative free energies obtained at the B3LYP-D3/TZVPP level. The calculated frequencies are listed in Tables S1 to S8 in the Supplementary Information.

1) Protonated systems

The calculations yield six LLH^+ structures with Gibbs free energy below 2 kcal/mol for LL and five for LDH^+. They all display a C5 interaction between $N_{(1)}H^+$ and $CO_{(1)}$. The two stable LL dipeptides which meet the requirements on both vibrational spectroscopy (Figure 3) and ion mobility are LL_{calc1} and LL_{calc2}. Both structures display a similar hydrogen bond pattern, with a strong ionic C5 interaction between $N_{(1)}H^+$ and $CO_{(1)}$ and a weak C'5 neutral hydrogen bond between the peptide $N_{(2)}H$ and the carboxylic $CO_{(2)}$. The structures involving an interaction between $N_{(1)}H^+$ and the carboxylic $CO_{(2)}$ are much higher in energy and have been discarded, as well as the structure where the NH^+…OC hydrogen bond is replaced by NH^+…aromatic ring interactions only.

While the C'5 neutral hydrogen bond between the peptide $N_{(2)}H$ and the carboxylic $CO_{(2)}$ is identical in LL_{calc1} and LL_{calc2} (2.40 vs. 2.42 Å, respectively), it is not the case for the strong interaction between $N_{(1)}H$ and $CO_{(1)}$. In LL_{calc1}, there is a compromise between the $N_{(1)}H^+…O_{(1)}$ and the $N_{(1)}H^+$…aromatic ring interaction. The resulting tradeoff leads to a quite large $N_{(1)}H^+…O_{(1)}$ distance (2.03 Å), while the two other NH occupy equivalent positions and bridge the two aromatic rings which are parallel to each other. In contrast in LL_{calc2}, $N_{(1)}H^+$ optimizes its interaction with $CO_{(1)}$, resulting in a closer $N_{(1)}H^+…O_{(1)}$ distance (1.73 Å) and a larger distance between the aromatic rings which adopt a "V" shape. Although both satisfactorily match the experimental data, we tend to favour LL_{calc1} for energetic reasons as it is lies 3.2 kcal/mol lower in energy, at the B3LYP-D3 level.

The cross section of the selected protonated LD_{calc} structure amounts to 110 Å². This structure shows a very strong ionic $N_{(1)}H^+…O_{(1)}$ bond (1.73Å) and no neutral C'5 $N_{(2)}H…O_{(2)}$ bond. The two aromatic rings are perpendicular to each other; it allows one of the ammonium $N_{(1)}H$ to interact with one of them and thereby compensates for the lack of neutral C'5.

The main difference between LL and LD (absence of neutral C'5 and perpendicular aromatic rings in LD) does not show clear vibrational signature. However, it manifests itself by a difference in drift time. Indeed, the theoretical results fairly well reproduce the fact that the collision cross section of LL (119 Å²) is slightly larger than that of LD (116 Å²).

2) Sodiated systems

The calculations yield three $LLNa^+$ structures with Gibbs free energy below 2 kcal/mol, which show either OOπ or Oππ interaction. The three calculated LD Na^+ structures are all of OOπ nature. The vibrational spectra of the sodiated dipeptides have been reported by Dunbar et al[39] together with calculations supporting the existence of a very stable OOπ form, common to the two diastereomers. The results presented here (Figure 4) parallel the latter results, as the very stable $LLNa^+_{calc1}$ possesses such a structure and has a satisfactory cross section of 115 Å². In $LLNa^+_{calc1}$, the interaction between the alkali and the CO groups is strong as indicated by a short distance, 2.21 and 2.27 Å for the amide and carboxyl CO, respectively. The Na^+…π distance is short too, 2.90 Å. The two aromatic rings are in an extended geometry and do not interact with each other. The structure displays a C'5 neutral hydrogen bond between the peptide $N_{(2)}H$ and the $N_{(1)}$ terminal. The second stable form compatible with the experimental results, namely $LLNa^+_{calc2,}$ is an Oππ structure in which the alkali interacts with the amide $CO_{(1)}$ (distance of 2.16 Å) and the two aromatic rings which are therefore kept parallel to each other. The peptide $N_{(2)}H$ is involved in a bifurcated C'5 neutral hydrogen bond involving both $N_{(1)}$ and the carboxylic $CO_{(2)}$. This structure is different from the NOπ structure proposed by Dunbar et al. [39] Indeed, both NOπ and Oππ structures account well for the high-energy shoulder of the band due to the CO stretch. However, the NOπ structure is calculated much higher in energy here (2.7 at the B3LYP-D3/TZVPP). Moreover, its calculated cross section amounts to 119 Å², which is larger than expected from the measurements.

The sodiated LD dipeptide stands out with the largest experimental cross section among all the dipeptides studied. Among the calculated sodiated LD dipeptides which reproduce well the experimental IRMPD spectrum (Figure 4), the $LDNa^+_{calc}$ of OOπ nature shown in Figure 7 has a calculated cross section the most compatible with the experiment. Its hydrogen bond pattern is similar to that observed in $LLNa^+_{calc1}$, with a distance between the alkali and the amide or carboxyl oxygens of 2.20 or 2.30 Å, respectively. The effect of chirality is that the $LDNa^+_{calc}$ differs from $LLNa^+_{calc1}$ by the outwards orientation of the aromatic ring, which explains the larger experimental and calculated cross section.

The results obtained here align with those previously reported; only one form of sodiated LD is observed in our experimental conditions while two forms coexist for LL. Moreover, the differences in experimental frequencies are qualitatively reproduced by the calculations; the NH band is red shifted and the OH bends blue shifted in $LDNa^+$.

II. Calculated structures of tetraphenylalanines

The assignment of the observed tetrapeptides to one or several of the calculated forms has been done following the same line as for the dipeptides. The selected structures are shown in Figure 8.

1) Protonated systems

The calculations yield two $LLLLH^+$ and seven $LDLDH^+$ structures with Gibbs free energy below 2 kcal/mol. Among the calculated structures, only two $LDLDH^+$ and one $LLLLH^+$ match the experimental spectra. They are further sorted out by their energy and mobility. The $LLLL_{calc}$ structure shown in Figure 8 presents satisfactory agreement with both the vibrational spectroscopy (Figure 5) and ion mobility results, and is the most stable at the B3LYP-D3/TZVPP level. This structure involves a strong C11 interaction between $N_{(1)}H_3^+$ and the C terminal $CO_{(3)}$, with a $N_{(1)}H^+\ldots O_{(3)}$ distance as short as 1.66 Å. The two other $N_{(1)}H^+$ are involved in interactions with the aromatic rings located on the C and N termini (α_1 and α_4 positions), with distances between $N_{(1)}H_3^+$ and the aromatic rings in α_1 and α_4 of 2.4 and 2.6 Å, respectively. The latter larger distance is due to the fact that the $N_{(1)}H^+$ interacting with the aromatic ring in α_4 position is also involved in a C5 ring with $CO_{(1)}$. These $N_{(1)}H+\ldots\pi$ interactions keep the two aromatic rings parallel, and make the structure rather compact, with a calculated cross section of 167 Å². The carboxylic acid group is directed outwards and only interacts with the rest of the molecule *via* its $CO_{(4)}$ involved as an acceptor in a neutral C'5 interaction with $N_{(4)}H$. The fact that the carboxylic group does not act as a hydrogen bond donor manifests itself by the value of the C-OH bend (1173 cm^{-1}).[49] Lastly, the other amide carbonyl $CO_{(2)}$ and the peptidic $N_{(2)}H$ are free.

$LDLD_{calc1}$ is the most stable LDLD structure; its collision cross section is also the most satisfactory. Its $N_{(1)}H_3^+$ is involved in a similar interaction pattern as in $LLLL_{calc}$, namely a C11 and two $NH^+\ldots\pi$. However, the rings involved in the interactions are not the same as in $LLLL_{calc}$, but are in α_1 and α_3 positions. $LDLD_{calc1}$ strongly differs from $LLLL_{calc}$ by the environment of the carboxylic acid. A C'11 interaction takes place between the carboxylic carbonyl $CO_{(4)}$ and the amide $N_{(2)}H$. This interaction is accompanied by a weak $C_{(4)}OH\ldots\pi$ interaction with the aromatic ring in α_2 position, with an $OH\ldots\pi$ distance of 2.58 Å. The spectroscopic fingerprint of this interaction is a blue shift of the C-OH bending mode which is calculated at 1199 cm^{-1}, as observed in sodiated polyglycines.[47] None of the CO or NH are free as two C'7 interactions take place between $C_{(2)}O\ldots HN_{(4)}$ and $C_{(1)}O\ldots HN_{(3)}$.

In $LDLD_{calc2}$, the $N_{(1)}H_3^+$ ammonium interacts with $C_{(3)}O$ and the aromatic ring in α_3, like in $LDLD_{calc1}$, but there is no interaction with another aromatic ring. The same C'11 and C'7 interactions are observed. LLLL and LDLD have the same experimental cross section, which should be reproduced by the calculation. In this respect, the $LDLD_{calc1}$ structure fits the experimental cross section better than $LDLD_{calc2}$, although both of them are satisfactory in terms of spectroscopy.

In conclusion, the LLLL and LDLD systems share in common a strong C11 interaction between $N_{(1)}H_3^+$ and $OC_{(3)}$, accompanied by NH_3^+…π interactions. They differ however by the nature of the aromatic rings involved in the NH_3^+…π interactions and by the neutral interactions, LLLL showing exclusively short-distance interactions like C'5 while LDLD shows long distance structuration like C'7 or C'11. The differences in experimental spectroscopy of protonated LLLL and LDLD is qualitatively reproduced by the calculations, in particular the more structured aspect of the NH bend region and the presence of an intense OH bend band in LLLL.

2) Sodiated systems

The calculations yield four $LLLLNa^+$ and seven $LDLDNa^+$ structures with Gibbs free energy below 2 kcal/mol. The low-energy calculated structures of $LLLLNa^+$ all display OOππ structures. Those with an OOOπ pattern are higher in energy by at least 1.6 kcal/mol. Among the OOππ structures, the $LLLLNa_{calc}^+$ shown in Figure 8 gives the best agreement with the experimental vibrational spectrum (Figure 6) and is the most stable. The sodium interacts with two carbonyl groups, namely $CO_{(1)}$ and $CO_{(3)}$, with distances as short as 2.18 Å. The carboxylic acid is directed outwards as does not interact with the sodium. The cation also interacts strongly with the terminal aromatic rings, as indicated by short distances of 2.9-3.1 Å between Na^+ and the benzene in α_1 or α_4. In contrast, the two other benzene rings in α_2 and α_3 are dangling; they interact much less with Na^+ (distances of ~5 Å) but adopt a parallel geometry which allows optimising dispersion. In addition, two neutral C'5 interactions are observed from $NH_{(2)}$ to $NH_{(1)}$ and from $N_{(4)}H$ to $CO_{(4)}$. The carboxyl, the $N_{(3)}H$ as well as the peptidic $CO_{(2)}$ groups are free.

All the $LDLDNa^+$ calculated structures in a 2 kcal/mol window display an OOOOπ structure, with the sodium interacting with the four CO as well as the aromatic ring in α_1. The $LDLDNa_{calc}^+$ structure compatible with both measured collision cross section and vibrational spectrum is shown in Figure 8, it is the second most stable of all calculated forms. The

$Na^+…O_{(1)}$, $Na^+…O_{(2)}$, $Na^+…O_{(3)}$, and $Na^+…O_{(4)}$ distances amount to 2.28, 2.20, and 2.56, and 2.39 Å, respectively; they are longer than in $LLLLNa_{calc}^+$. In contrast with $LLLLNa_{calc}^+$, only one aromatic ring interacts with the cation, with a distance between the phenyl and the cation of 3.08 Å. Among the neutral C'5 interactions observed in $LLLLNa_{calc}^+$, only that from $NH_{(2)}$ to $NH_{(1)}$ exists in $LDLDNa_{calc}^+$.

Discussion

We shall first compare the protonated systems studied here to the protonated phenylalanine monomer. The spectroscopy of protonated phenylalanine has been studied both in room temperature and cryogenic ion traps.[18] Two conformers have been evidenced, which show different IR signatures[76] as well as different dynamics in the first electronic excited state.[77] They both display a C5 $NH_3^+…O$ hydrogen-bond and an $NH_3^+…\pi$ interaction with the aromatic ring and only differ in the orientation of the amino-acid backbone relative to the aromatic ring. This pattern is retained in both protonated dipeptides. In the protonated tetrapeptides, the aromatic ring in α_1 competes with remote aromatic rings for interacting with the charged NH_3^+. The resulting trade-off is a bifurcated interaction involving Phe(α_1) and Phe(α_4) for $LLLL_{calc}$. In the $LDLDH_{calc}^+$ structures, the remote aromatic ring involved in this competition is Phe(α_3). A bifurcated interaction takes place between Phe(α_1) and Phe(α_3) for $LDLD_{calc1}$ while NH_3^+ interacts only with Phe(α_3) in $LDLD_{calc2}$.

Another interesting aspect is to assess the role of the aromatic ring in the structure of the protonated peptides. The IRMPD spectrum of protonated Ala_n has been interpreted thanks to Car-Parrinello molecular dynamics at 300 K.[45] The results show that protonated Ala_2 spends most of the time in a trans configuration with $NH^+…O$ (C5) and NH…OCOH (C'5) interactions, which is similar to that observed in protonated LL. In LD however, no C'5 interaction takes place. Ion mobility[78] as well as vibrational spectroscopy of photochemically-produced protonated Ala_4[79] have suggested that it adopts a folded structure in which the protonated N terminal is involved in a C8 interaction possibly accompanied by a C11 interaction with the carboxylic acid. The terapeptides studied here do not show this long-distance structuration but retain the $NH^+…O$ (C5) pattern observed in protonated dialanine or diphenylalanine, probably because the long-distance structuration is prevented by the bulkiness of the aromatic ring and the NH…π interactions. The two protonated tetraphenylalanines show differences in their neutral interactions (C'5 for LLLL and C'7 or C'11 for LDLD). It is to be stressed here that the strong C5 ionic interactions is common to all

the studied protonated peptides and that the sensitivity to chirality depends on much weaker neutral interactions.

Sodiated peptides raise the question of the competition between O and N as the interaction sites. For example, the IRMPD spectrum of Ala_2Na^+ is compatible with a OO structure, possibly accompanied by an additional interaction with NH_2.[49] As in most of the cationised peptide studied, the carboxylic acid interacts with Na^+ through its carbonyl. The structuring effect of Na^+ is also evidenced in Ala_3Na^+ in which the charge is fully solvated by the three carbonyls.[49] Despite the fact that no experimental spectroscopic data is available for Ala_4Na^+, Na^+ sits on top of the oxygens of three nearly parallel CO in its most stable calculated form, the structure being closed by the hydrogen bonding interaction between the two C and N termini. However, the structure in which Na^+ interacts with the four CO is not much higher in energy.[80]

The presence of an aromatic ring adds a third site. Indeed, cationised phenylalanine, $PheNa^+$, shows a charge-solvated ONπ structure.[81] However, this structure is given up in the diphenylalanines studied here to the benefit of OOπ or Oππ structures. It should be mentioned that the structure responsible for the blue shoulder of the CO stretch band has been assigned to an ONπ structure by Dunbar et al., which contrasts with our assignment to an Oππ form. The difference in energy between ONπ and Oππ structures might depend on the computational method used.

The IRMPD spectra of $AlaPheNa^+$ and $PheAlaNa^+$ have been explained in terms of the coexistence of OOπ and ONπ forms involving the C terminus and the amide NH or the amide CO and NH_2. OOπ and OOππ are proposed for $PhePheNa^+$ and $PhePheK^+$. [50] OONππ are observed for divalent ions such as Ni^{2+}.[82] The presence of a second aromatic ring seems therefore to exclude interaction with N in natural aminoacids.

In the tetrapeptides as well, the important aspect is the competition between O and π for solvating the cation. This competition depends on chirality as OOππ is observed in LLLL in contrast with OOOOπ in LDLD, with a wrapped structure. The quantum chemical method should be carefully chosen to be able to reproduce the equulibrium between the physical effects involved in these manifold structures.

Conclusion

IRMPD and ion mobility spectrometry are complementary methods for structural characterization of di- or tetra-phenylalanines composed of residues of identical or alternating

chirality. While IRMPD is sensitive to the hydrogen bond network that stabilizes the structure, IMS gives information of the global shape of the molecule. The only difference between LDH^+ and LLH^+ was found to be the presence of a neutral C'5 in the former, which has only limited consequences such as slightly different vibrational transition intensity and collision cross sections. This system confirms the previous hypothesis that the interaction responsible for chiral differentiation, here the neutral C'5, may be much weaker than the main ionic interaction. [22] Two isomers of $LLNa^+$ are formed, namely OOπ and Oππ with different spectroscopic signatures. This conclusion differs from that of Dunbar *et al.* who suggested OOπ and ONπ conformers.[39] In contrast, $LDNa^+$ exists in one OOπ isomer only, with cross section much larger than that of $LLNa^+$. The competition between Na^+…O and Na^+…π interactions strongly depend on chirality.

Although the binding pattern changes from OOππ in $LLLLNa^+$ to OOOOπ in $LDLDNa^+$, neither the spectroscopic signature nor the collision cross section is strongly affected by the chirality of the residues in the sodiated tetrapeptides. In contrast, $LLLLH^+$ and $LDLDH^+$ show different spectroscopic signatures explained in terms different secondary NH^+…π interactions.

The spectra simulated on the basis of harmonic frequencies lead to satisfactory agreement with the experimental values. Quantum chemical calculations have provided low-energy structures with a size compatible with IMS measurements. However, molecular dynamics calculations would bring interesting information on these highly flexible systems.[83] Those resting on a well-adapted polarizable force field are especially promising for molecules of this size.[84]

The structural differences induced by chirality should manifest itself in the aggregation properties. Conformer-specific studies at low temperature of these systems would bring interesting information, especially in the UV range. Specific photofragments as a function of the residues chirality could be searched for.[77, 85, 86]

Acknowledgment

The mass spectrometry platform SMAS of the Laboratoire de Chimie Physique (University Paris-Sud) is gratefully acknowledged. We thank Dr. J. M. Ortega and the CLIO team for technical assistance. We acknowledge V. Steinmetz for his assistance in the experimental work. We acknowledge the use of the computing facility cluster GMPCS of the LUMAT federation (FR LUMAT 2764) and of the DI Univ. Paris-Sud.

Figure captions

Table 1. Relative free energies (kcal/mol) at the B3LYP-D3/TZVPP level together with experimental and calculated (at the B3LYP-D3/TZVPP geometries) collision cross sections (Å²) of the studied systems.

Figure 1: Scheme of the molecules under study and numbering of atoms. The chiral centers are indicated by * (top). Fragmentation pattern of the studied peptides (bottom).

Figure 2: Mass spectra of an acidified a) dipeptides and b) tetrapeptides solution.

Figure 3: IRMPD Experimental spectrum of protonated LL and LD together with the simulated spectra of LL_{calc2}, $LL_{calc1,}$ LD_{calc}. The B3LYP-D3/TZVPP harmonic frequencies are scaled by 0.98.

Figure 4: IRMPD Experimental spectrum of sodiated LL and LD together with the simulated spectra of $LLNa^{+}_{calc1,}$ $LLNa^{+}_{calc2}$ and $LDNa_{calc}^{+}$. The B3LYP-D3/TZVPP harmonic frequencies are scaled by 0.98.

Figure 5: Experimental spectrum of protonated LLLL and LDLD together with the simulated spectra of $LLLL_{calc}$, $LDLD_{calc1}$ and $LDLD_{calc2}$. The B3LYP-D3/TZVPP harmonic frequencies are scaled by 0.98.

Figure 6: Experimental spectrum of a) sodiated LLLL b) sodiated LDLD together with the simulated spectra of b) $LLLLNa_{calc}^{+}$ d) $LDLDNa_{calc}^{+}$. The B3LYP-D3/TZVPP harmonic frequencies are scaled by 0.98.

Figure 7: Calculated structures assigned to the experimentally observed diphenylalanines.

Figure 8: Calculated structures assigned to the experimentally observed tetraphenylalanines.

References

1. A. Zehnacker, ed., *Chiral recognition in the Gas Phase*, CRC Press Taylor & Francis Group, Boca Raton, 2010.
2. M. Albrecht, A. Borba, K. Le Barbu-Debus, B. Dittrich, R. Fausto, S. Grimme, A. Mahjoub, M. Nedic, U. Schmitt, L. Schrader, M. A. Suhm, A. Zehnacker-Rentien and J. Zischang, *New Journal of Chemistry*, 2010, **34**, 1266-1285.
3. A. Zehnacker and M. A. Suhm, *Angewandte Chemie-International Edition*, 2008, **47**, 6970-6992.
4. N. Borho and M. A. Suhm, *Physical Chemistry Chemical Physics*, 2002, **4**, 2721-2732.
5. N. Borho and M. A. Suhm, *Physical Chemistry Chemical Physics*, 2004, **6**, 2885-2890.
6. A. Giardini-Guidoni, A. Paladini, F. Rondino, S. Piccirillo, M. Satta and M. Speranza, *Organic & Biomolecular Chemistry*, 2005, **3**, 3984-3989.
7. A. Latini, D. Toja, A. Giardini-Guidoni, S. Piccirillo and M. Speranza, *Angewandte Chemie-International Edition*, 1999, **38**, 815-817.
8. Z. Su, N. Borho and Y. J. Xu, *Journal of the American Chemical Society*, 2006, **128**, 17126-17131.
9. J. Thomas, F. X. Sunahori, N. Borho and Y. Xu, *Chemistry-a European Journal*, 2011, **17**, 4582-4587.
10. N. Seurre, J. Sepiol, K. Le Barbu-Debus, F. Lahmani and A. Zehnacker-Rentien, *Physical Chemistry Chemical Physics*, 2004, **6**, 2867-2877.
11. K. Le Barbu-Debus, M. Broquier, A. Mahjoub and A. Zehnacker-Rentien, *Physical Chemistry Chemical Physics*, 2009, **11**, 7589-7598.
12. R. Thissen, O. Dutuit, C. Alcaraz, O. Laprevote, L. Serani, P. Millie and J. M. Soudan, *Physical Chemistry Chemical Physics*, 2002, **4**, 661-667.
13. R. G. Cooks and P. S. H. Wong, *Accounts of Chemical Research*, 1998, **31**, 379-386.
14. B. L. Young and R. G. Cooks, *International Journal of Mass Spectrometry*, 2007, **267**, 199-204.
15. W. A. Tao and R. G. Cooks, *Analytical Chemistry*, 2003, **75**, 25A-31A.
16. S. Ahn, J. Ramirez, G. Grigorean and C. B. Lebrilla, *Journal of the American Society for Mass Spectrometry*, 2001, **12**, 278-287.
17. C. Fraschetti, M. Pierini, C. Villani, F. Gasparrini, A. Filippi and M. Speranza, *Collection of Czechoslovak Chemical Communications*, 2009, **74**, 275-297.
18. R. H. Wu and T. B. McMahon, *Chemphyschem*, 2008, **9**, 2826-2835.
19. P. Dwivedi, C. Wu, L. M. Matz, B. H. Clowers, W. F. Siems and H. H. Hill, *Analytical Chemistry*, 2006, **78**, 8200-8206.
20. F. X. Sunahori, G. Yang, E. N. Kitova, J. S. Klassen and Y. Xu, *Physical Chemistry Chemical Physics*, 2013, **15**, 1873-1886.
21. A. Filippi, C. Fraschetti, S. Piccirillo, F. Rondino, B. Botta, I. D'Acquarica, A. Calcaterra and M. Speranza, *Chemistry-a European Journal*, 2012, **18**, 8320-8328.
22. D. Scuderi, K. Le Barbu-Debus and A. Zehnacker, *Physical Chemistry Chemical Physics*, 2011, **13**, 17916-17929.
23. A. Sen, K. Le Barbu-Debus, D. Scuderi and A. Zehnacker-Rentien, *Chirality*, 2013, **25**, 436-443.
24. D. Scuderi, P. Maitre, F. Rondino, K. Le Barbu-Debus, V. Lepere and A. Zehnacker-Rentien, *Journal of Physical Chemistry A*, 2010, **114**, 3306-3312.

25. A. G. Abo-Riziq, J. E. Bushnell, B. Crews, M. P. Callahan, L. Grace and M. S. de Vries, *International Journal of Quantum Chemistry*, 2005, **105**, 437-445.
26. A. Mahjoub, A. Chakraborty, V. Lepere, K. Le Barbu-Debus, N. Guchhait and A. Zehnacker, *Physical Chemistry Chemical Physics*, 2009, **11**, 5160-5169.
27. J. C. Dean, E. G. Buchanan, W. H. James, A. Gutberlet, B. Biswas, P. V. Ramachandran and T. S. Zwier, *Journal of Physical Chemistry A*, 2011, **115**, 8464-8478.
28. M. E. Crestoni, B. Chiavarino, D. Scuderi, A. Di Marzio and S. Fornarini, *Journal of Physical Chemistry B*, 2012, **116**, 8771-8779.
29. A. Bouchet, J. Klyne, G. Piani, O. Dopfer and A. Zehnacker, *Physical Chemistry Chemical Physics*, 2015, **17**, 25809-25821.
30. E. Gloaguen, F. Pagliarulo, V. Brenner, W. Chin, F. Piuzzi, B. Tardivel and M. Mons, *Physical Chemistry Chemical Physics*, 2007, **9**, 4491-4497.
31. A. Sen, A. Bouchet, V. Lepere, K. Le Barbu-Debus, D. Scuderi, F. Piuzzi and A. Zehnacker-Rentien, *The Journal of Physical Chemistry. A*, 2012, **116**, 8334-8344.
32. A. Sen, V. Lepere, K. Le Barbu-Debus and A. Zehnacker, *Chemphyschem : a European Journal of Chemical Physics and Physical Chemistry*, 2013, **14**, 3559-3568.
33. C. D. Drew, G. T. Knight, D. T. Hughes and M. Bush, *British Journal of Clinical Pharmacology*, 1978, **6**, 221-225.
34. P. Butz, R. T. Kroemer, N. A. Macleod, E. G. Robertson and J. P. Simons, *Journal of Physical Chemistry A*, 2001, **105**, 1050-1056.
35. C. J. Saavedra, A. Boto, R. Hernandez, J. I. Miranda and J. M. Aizpurua, *Journal of Organic Chemistry*, 2012, **77**, 5907-5913.
36. C. M. Adams, F. Kjeldsen, R. A. Zubarev, B. A. Budnik and K. F. Haselmann, *Journal of the American Society for Mass Spectrometry*, 2004, **15**, 1087-1098.
37. R. Sudha and M. F. Jarrold, *Journal of Physical Chemistry B*, 2005, **109**, 11777-11780.
38. R. C. Dunbar, J. D. Steill and J. Oomens, *International Journal of Mass Spectrometry*, 2010, **297**, 107-115.
39. R. C. Dunbar, J. D. Steill and J. Oomens, *Journal of the American Chemical Society*, 2011, **133**, 1212-1215.
40. E. Gloaguen, H. Valdes, F. Pagliarulo, R. Pollet, B. Tardivel, P. Hobza, F. Piuzzi and M. Mons, *The Journal of Physical Chemistry A*, 2009, **114**, 2973-2982.
41. R. Wu and T. B. McMahon, *Journal of the American Chemical Society*, 2007, **129**, 11312-11313.
42. A. Sediki, L. C. Snoek and M. P. Gaigeot, *International Journal of Mass Spectrometry*, 2011, **308**, 281-288.
43. C. M. Leavitt, A. F. DeBlase, C. J. Johnson, M. van Stipdonk, A. B. McCoy and M. A. Johnson, *Journal of Physical Chemistry Letters*, 2013, **4**, 3450-3457.
44. G. Gregoire, M. P. Gaigeot, D. C. Marinica, J. Lemaire, J. P. Schermann and C. Desfrancois, *Physical Chemistry Chemical Physics*, 2007, **9**, 3082-3097.
45. D. C. Marinica, G. Gregoire, C. Desfrancois, J. P. Schermann, D. Borgis and M. P. Gaigeot, *Journal of Physical Chemistry A*, 2006, **110**, 8802-8810.
46. J. K. Martens, I. Compagnon, E. Nicol, T. B. McMahon, C. Clavaguera and G. Ohanessian, *Journal of Physical Chemistry Letters*, 2012, **3**, 3320-3324.
47. O. P. Balaj, D. Semrouni, V. Steinmetz, E. Nicol, C. Clavaguera and G. Ohanessian, *Chemistry-a European Journal*, 2012, **18**, 4583-4592.
48. D. Semrouni, O. P. Balaj, F. Calvo, C. F. Correia, C. Clavaguera and G. Ohanessian, *Journal of the American Society for Mass Spectrometry*, 2010, **21**, 728-738.

49. O. P. Balaj, C. Kapota, J. Lemaire and G. Ohanessian, *International Journal of Mass Spectrometry*, 2008, **269**, 196-209.
50. R. C. Dunbar, J. D. Steill and J. Oomens, *Journal of the American Chemical Society*, 2011, **133**, 9376-9386.
51. J. C. Poully, F. Lecomte, N. Nieuwjaer, B. Manil, J. P. Schermann, C. Desfrancois, G. Gregoire, R. Ballivian, F. Chirot, J. Lemoine, F. Calvo, R. Antoine and P. Dugourd, *International Journal of Mass Spectrometry*, 2010, **297**, 28-35.
52. F. Albrieux, F. Calvo, F. Chirot, A. Vorobyev, Y. O. Tsybin, V. Lepere, R. Antoine, J. Lemoine and P. Dugourd, *Journal of Physical Chemistry A*, 2010, **114**, 6888-6896.
53. P. Dugourd, R. R. Hudgins, D. E. Clemmer and M. F. Jarrold, *Review of Scientific Instruments*, 1997, **68**, 1122-1129.
54. M. Kohtani, T. C. Jones, R. Sudha and M. F. Jarrold, *Journal of the American Chemical Society*, 2006, **128**, 7193-7197.
55. E. S. Baker, S. L. Bernstein, V. Gabelica, E. De Pauw and M. T. Bowers, *International Journal of Mass Spectrometry*, 2006, **253**, 225-237.
56. E. R. Badman, S. Myung and D. E. Clemmer, *Journal of the American Society for Mass Spectrometry*, 2005, **16**, 1493-1497.
57. M. G. Krone, A. Baumketner, S. L. Bernstein, T. Wyttenbach, N. D. Lazo, D. B. Teplow, M. T. Bowers and J. E. Shea, *Journal of Biomedical Science*, 2008, **381**, 221-228.
58. B. T. Ruotolo, K. Giles, I. Campuzano, A. M. Sandercock, R. H. Bateman and C. V. Robinson, *Science*, 2005, **310**, 1658-1661.
59. M. K. Drayß, D. Blunk, J. Oomens, N. Polfer, C. Schmuck, B. Gao, T. Wyttenbach, M. T. Bowers and M. Schäfer, *International Journal of Mass Spectrometry*, 2009, **281**, 97-100.
60. L. Joly, R. Antoine, F. Albrieux, R. Ballivian, M. Broyer, F. Chirot, J. Lemoine, P. Dugourd, C. Greco, R. Mitrić and V. Bonačić-Koutecký, *The Journal of Physical Chemistry B*, 2009, **113**, 11293-11300.
61. B. Bellina, I. Compagnon, L. MacAleese, F. Chirot, J. Lemoine, P. Maitre, M. Broyer, R. Antoine, A. Kulesza, R. Mitric, V. Bonacic-Koutecky and P. Dugourd, *Physical Chemistry Chemical Physics*, 2012, **14**, 11433-11440.
62. L. Mac Aleese, A. Simon, T. B. McMahon, J.-M. Ortega, D. Scuderi, J. Lemaire and P. Maître, *International Journal of Mass Spectrometry*, 2006, **249-250**, 14-20.
63. J. M. Bakker, T. Besson, J. Lemaire, D. Scuderi and P. Maitre, *Journal of Physical Chemistry A*, 2007, **111**, 13415-13424.
64. H. E. Revercomb and E. A. Mason, *Analytical Chemistry*, 1975, **47**, 970-983.
65. *MacroModel version 9.8; ed. Schrödinger, LLC: New York, NY, 2010*, 2010.
66. J. Altnoeder, A. Bouchet, J. J. Lee, K. E. Otto, M. A. Suhm and A. Zehnacker-Rentien, *Physical Chemistry Chemical Physics*, 2013, **15**, 10167-10180.
67. D. Semrouni, C. Clavaguera, J. P. Dognon and G. Ohanessian, *International Journal of Mass Spectrometry*, 2010, **297**, 152-161.
68. M. D. Halls, J. Velkovski and H. B. Schlegel, *Theoretical Chemistry Accounts*, 2001, **105**, 413.
69. S. Grimme, J. Antony, S. Ehrlich and H. Krieg, *Journal of Chemical Physics*, 2010, **132**.
70. S. Grimme, S. Ehrlich and L. Goerigk, *Journal of Computational Chemistry*, 2011, **32**, 1456-1465.
71. R. Ahlrichs, M. Bar, M. Haser, H. Horn and C. Kolmel, *Chemical Physics Letters* 1989, **162**, 165-169.

72. M. J. Frisch, G. W. Trucks, H. B. Schlegel, G. E. Scuseria, M. A. Robb, J. R. Cheeseman, G. Scalmani, V. Barone, B. Mennucci, G. A. Petersson, H. Nakatsuji, M. Caricato, X. J. Li, H. P. Hratchian, A. F. Izmaylov, J. Bloino, G. Zheng, J. L. Sonnenberg, M. Hada, M. Ehara, K. Toyota, R. Fukuda, J. Hasegawa, M. Ishida, T. Nakajima, Y. Honda, O. Kitao, H. Nakai, T. Vreven, J. Montgomery, J. A. , J. E. Peralta, F. Ogliaro, M. Bearpark, J. J. Heyd, E. Brothers, K. N. Kudin, V. N. Staroverov, R. Kobayashi, J. Normand, K. Raghavachari, A. Rendell, J. C. Burant, S. S. Iyengar, J. Tomasi, M. Cossi, N. Rega, J. M. Millam, M. Klene, J. E. Knox, J. B. Cross, V. Bakken, C. Adamo, J. Jaramillo, R. Gomperts, R. E. Stratmann, O. Yazyev, A. J. Austin, R. Cammi, C. Pomelli, J. W. Ochterski, R. L. Martin, K. Morokuma, V. G. Zakrzewski, G. A. Voth, P. Salvador, J. J. Dannenberg, S. Dapprich, A. D. Daniels, O. Farkas, J. B. Foresman, J. V. Ortiz, J. Cioslowski and D. J. S. Fox, *Journal*, 2009, Gaussian 09, Revision A.02.
73. M. F. Mesleh, J. M. Hunter, A. A. Shvartsburg, G. C. Schatz and M. F. Jarrold, *Journal of Physical Chemistry*, 1996, **100**, 16082-16086.
74. P. Parneix, M. Basire and F. Calvo, *Journal of Physical Chemistry A*, 2013, **117**, 3954-3959.
75. J. Y. Salpin and D. Scuderi, *Rapid Communications in Mass Spectrometry*, 2015, **29**, 1-7.
76. J. A. Stearns, S. Mercier, C. Seaiby, M. Guidi, O. V. Boyarkin and T. R. Rizzo, *Journal of the American Chemical Society*, 2007, **129**, 11814-11820.
77. G. Feraud, M. Broquier, C. Dedonder, C. Jouvet, G. Gregoire and S. Soorkia, *The Journal of Physical Chemistry A*, 2015, **119**, 5914-5924.
78. R. R. Hudgins, Y. Mao, M. A. Ratner and M. F. Jarrold, *Biophysical Journal*, 1999, **76**, 1591-1597.
79. T. D. Vaden, T. de Boer, J. P. Simons, L. C. Snoek, S. Suhai and B. Paizs, *Journal of Physical Chemistry A*, 2008, **112**, 4608-4616.
80. P. Wang, C. Wesdemiotis, C. Kapota and G. Ohanessian, *Journal of the American Society for Mass Spectrometry*, 2007, **18**, 541-552.
81. R. C. Dunbar, J. D. Steill and J. Oomens, *Physical Chemistry Chemical Physics*, 2010, **12**, 13383-13393.
82. R. C. Dunbar, J. D. Steill, N. C. Polfer, G. Berden and J. Oomens, *Angewandte Chemie-International Edition*, 2012, **51**, 4591-4593.
83. J. Mahé, S. Jaeqx, A. M. Rijs and M. P. Gaigeot, *Physical Chemistry Chemical Physics*, 2015, **17**, 25905-25914.
84. F. Thaunay, J. P. Dognon, G. Ohanessian and C. Clavaguéra, *Phys. Chem. Chem. Phys.*, 2015, **17**, 25968-25977.
85. L. Voronina and T. R. Rizzo, *Physical Chemistry Chemical Physics*, 2015, **17**, 25828-25836.
86. G. Feraud, C. Dedonder, C. Jouvet, Y. Inokuchi, T. Haino, R. Sekiya and T. Ebata, *Journal of Physical Chemistry Letters*, 2014, **5**, 1236-1240.

Table 1. Relative free energies (kcal/mol) at the B3LYP-D3/TZVPP level together with experimental and calculated (at the B3LYP-D3/TZVPP geometries) collision cross sections (Å²) of the studied systems.

	ΔG (kcal/mol)	**Calculated cross section (Å²)**	**Experimental cross section (Å²)**
LLH$^+$			119
LL$_{calc1}$	0.0	115	-
LL$_{calc2}$	3.2	113	-
LDH$^+$			116
LD$_{calc}$		111	-
LLNa$^+$			116
LLNa$^+_{calc1}$	0.0	115	-
LLNa$^+_{calc2}$	0.3	112	-
LDNa$^+$			124
LD$_{calc}$	0.3	118	-
LLLLH$^+$			178
LLLL$_{calc}$	0.0	167	-
LDLDH$^+$			179
LDLD$_{calc1}$	0.0	168	-
LDLD$_{calc2}$	0.7	162	-
LLLLNa$^+$			183
LLLLNa$^+_{calc}$	0.0	174	-
LDLDNa$^+$			188
LDLDNa$^+_{calc}$	0.0	184	-

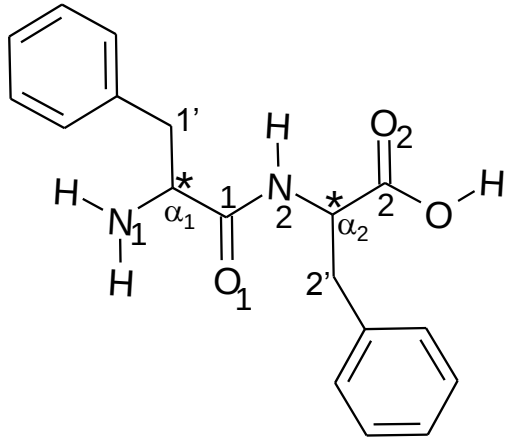

Diphenylalanines

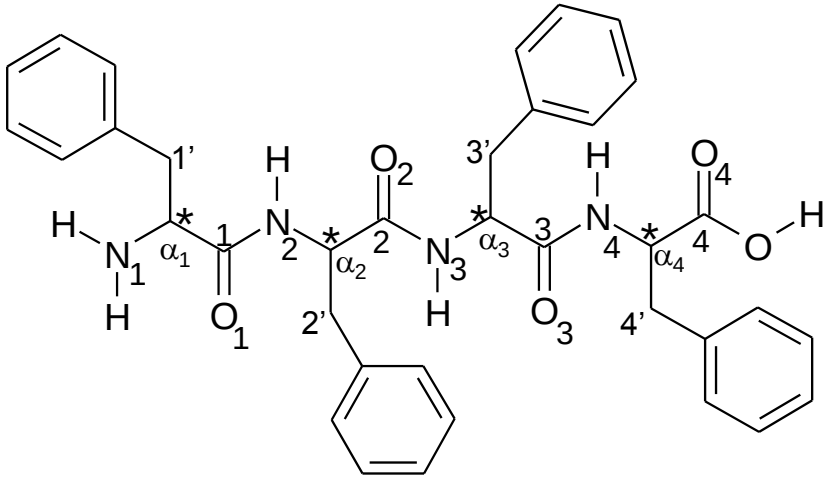

Tetraphenylalanines

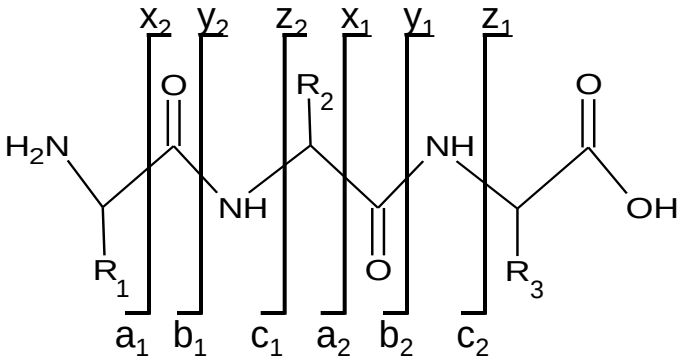

Dissociation pattern of peptides

Figure 1

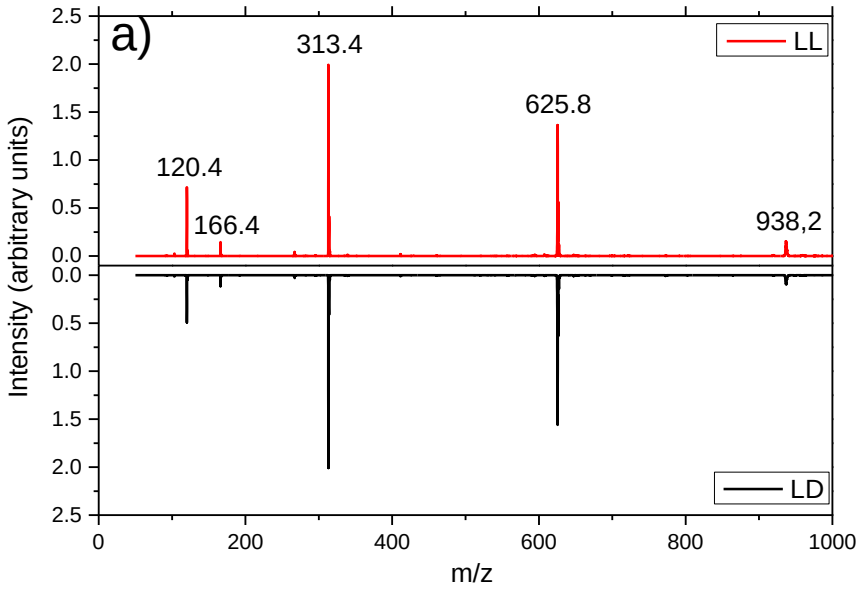

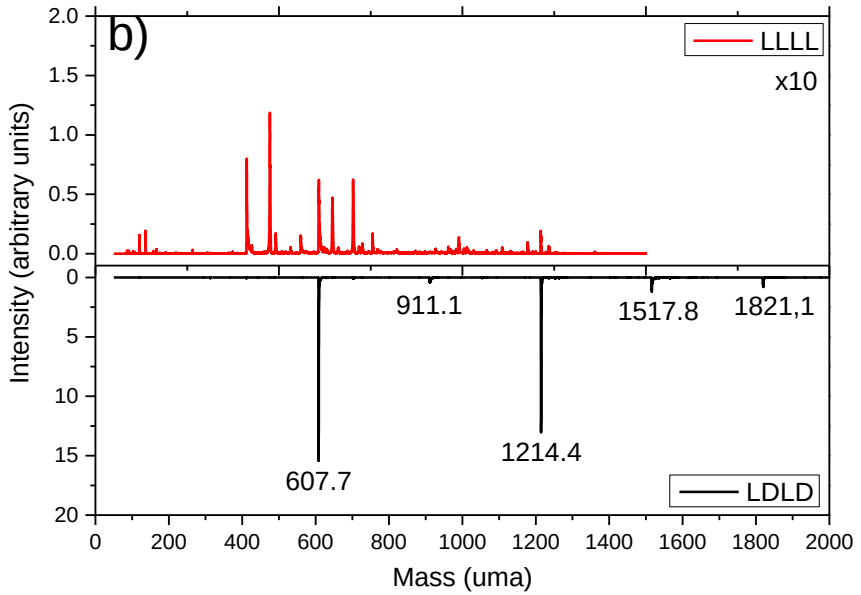

Figure 2

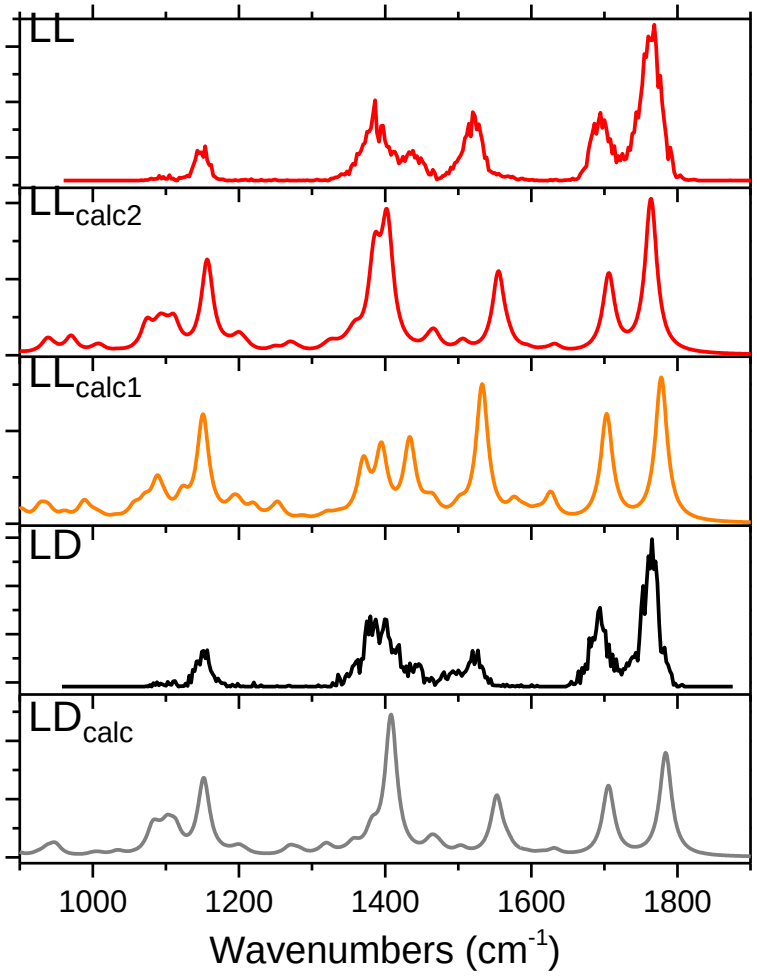

Figure 3

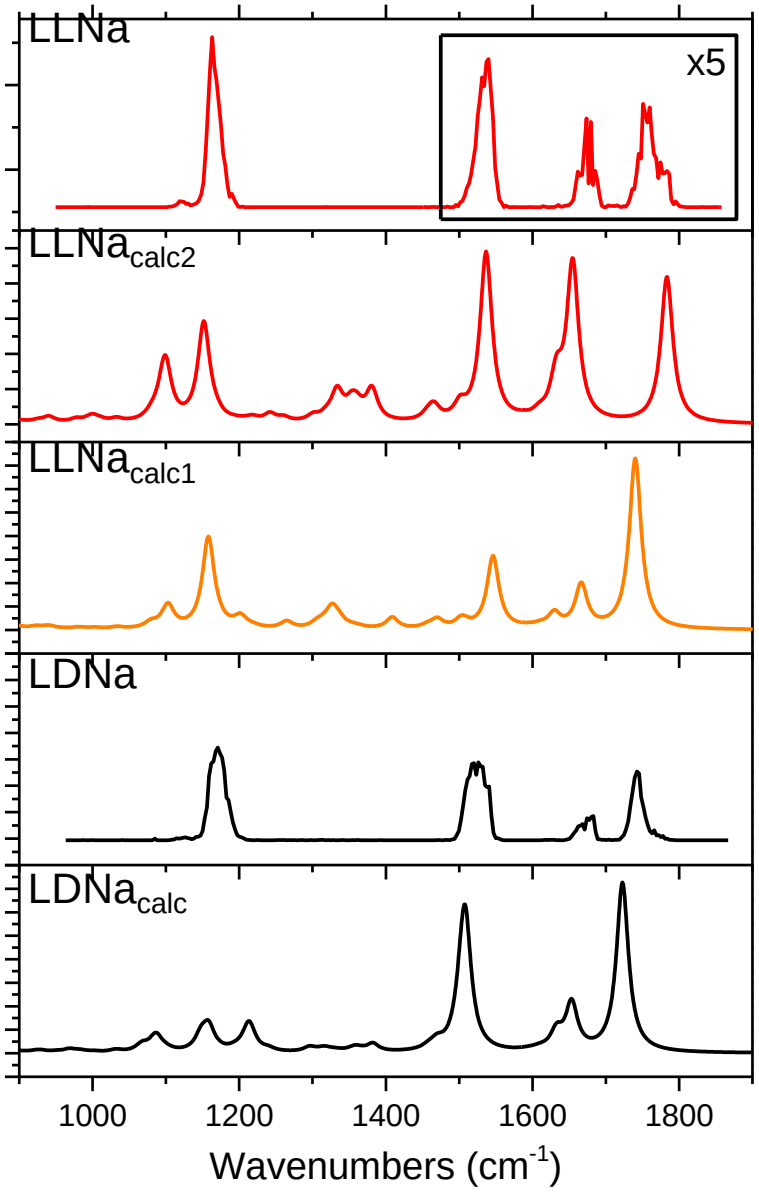

Figure 4

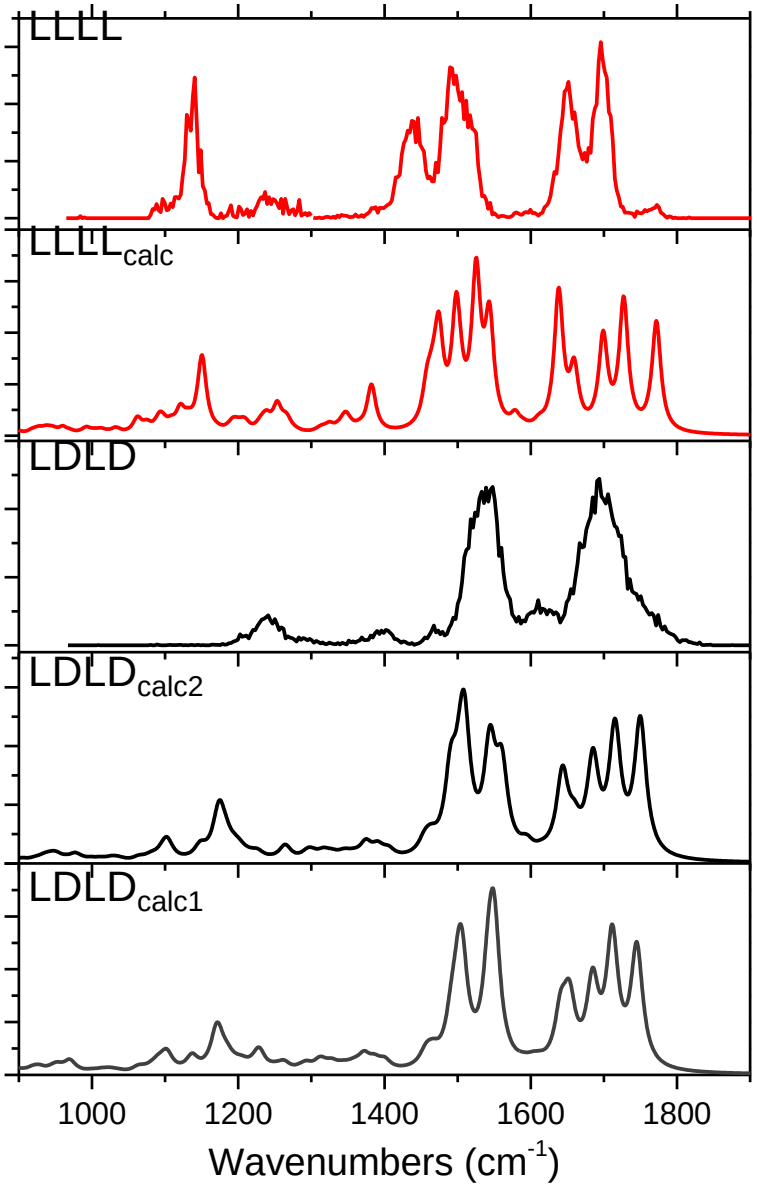

Figure 5

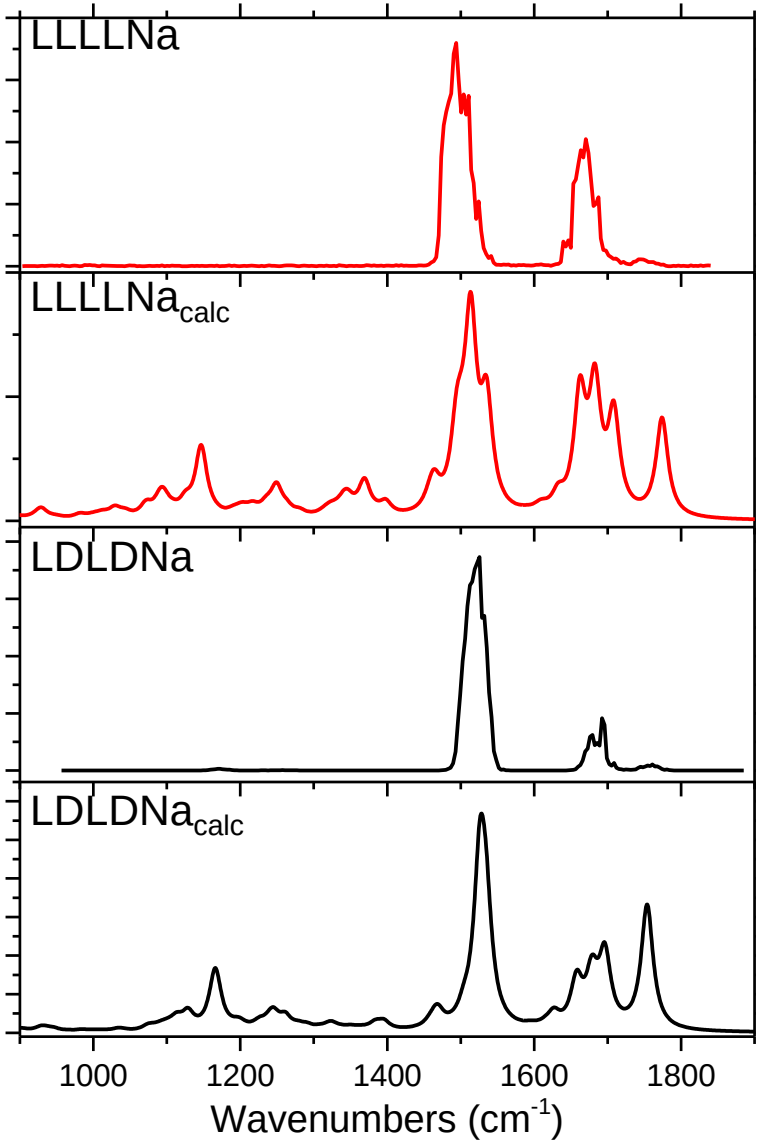

Figure 6

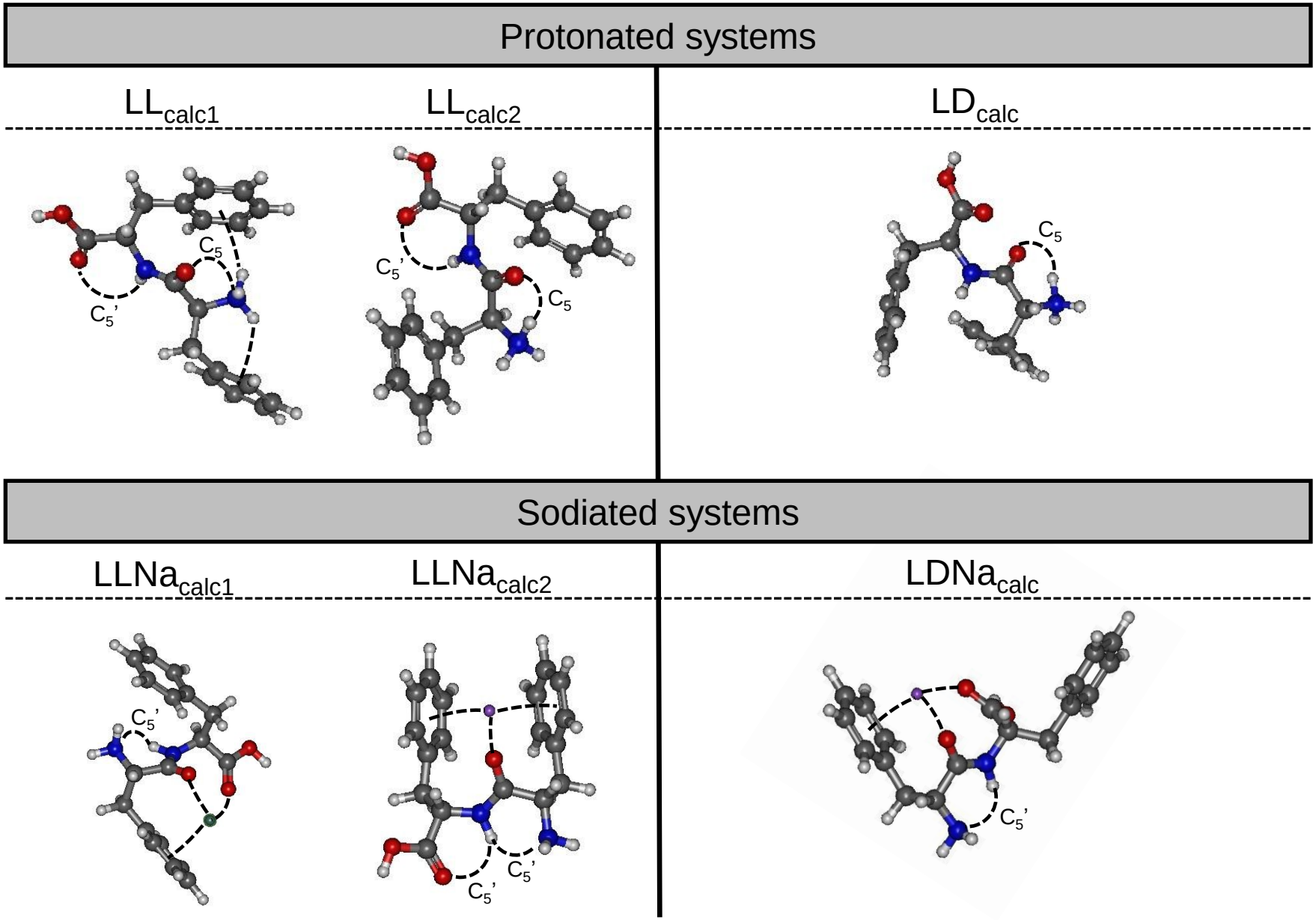

Figure 7

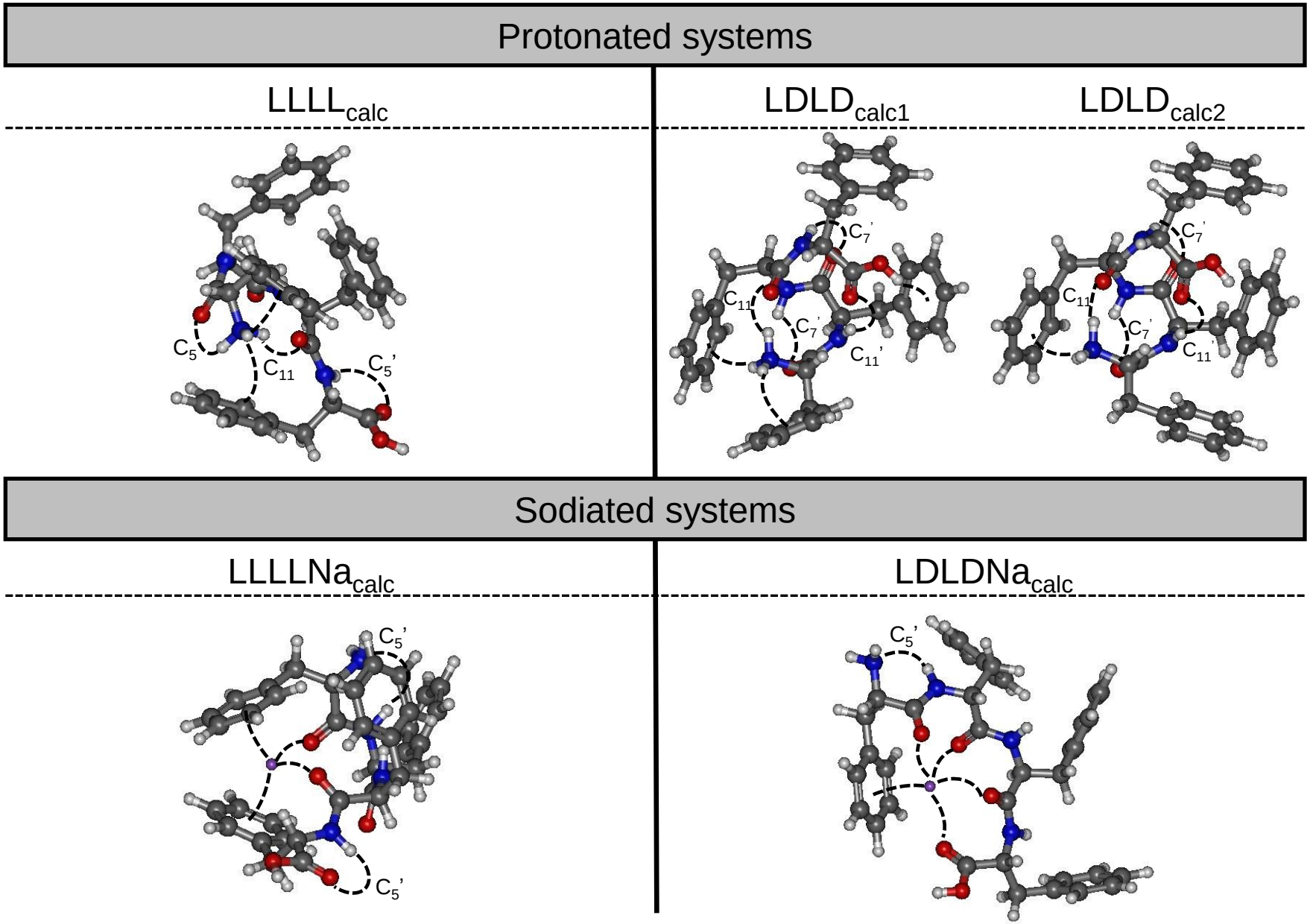

Figure 8

L-Phe-L-Phe-L-Phe-L-Phe-Na^+ / L-Phe-D-Phe-L-Phe-D-Phe-Na^+

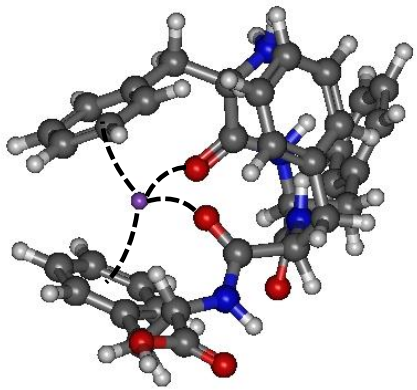

vs

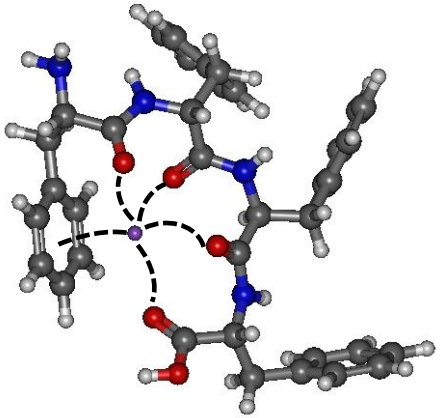

$Na^+ \ldots \pi$ * **2**
$Na^+ \ldots OC$ * **2**

$Na^+ \ldots \pi$ * **1**
$Na^+ \ldots OC$ * **4**

Graphical abstract